IEEE Access
Multidisciplinary | Rapid Review | Open Access Journal

Received November 30, 2020, accepted December 26, 2020, date of publication December 30, 2020,
date of current version January 7, 2021.

Digital Object Identifier 10.1109/ACCESS.2020.3048001

Analysis and Optimal Design of a Novel Actuator System for a Camera Module

TAE-HOON KWON AND JONG-SUK RO
Department of Electronic and Electrical Engineering, Chung-Ang University, Seoul 06974, South Korea

Corresponding author: Jong-Suk Ro (jongsukro@gmail.com)

This research was funded and conducted under the Competency Development Program for Industry Specialists of the Korean Ministry of Trade, Industry and Energy (MOTIE), operated by Korea Institute for Advancement of Technology (KIAT) (No. P0002397, HRD program for Industrial Convergence of Wearable Smart Devices), and was supported by the Chung-Ang University Research Scholarship Grants in 2019.

ABSTRACT Owing to the fourth industrial revolution and the recent trend for compact, high-performance, and multifunctional electrical devices, the demand for a small and high-performance camera module has dramatically increased. To address this, in this study, a novel, miniaturized, high-performance, low-cost multifunctional camera module with optical image stabilization (OIS) via a novel two-axis motional actuator with 1-Stage is proposed. To date, a systematic analysis and optimal design method for the actuators of camera modules has not been proposed yet. Accurate and rapid analysis and optimal design methods are proposed herein. Based on the proposed methods, it is possible to reduce the time and cost for the development of actuators for camera modules. The usefulness of the proposed actuator system for small, high performance, and multifunctional camera modules, and the proposed analysis and optimal design method were verified experimentally in this study.

INDEX TERMS Actuator, chamfered magnet, coil diameter, optical image stabilization (OIS), optimization algorithm, voice coil motor (VCM).

I. INTRODUCTION

The voice-coil-motor (VCM) type and the borrowed VCM actuator are the key components that are now used in camera modules represented by smartphones and digital single-lens reflex (DSLR) cameras that convert electronic and electrical signals (power) generated within the module into mechanical movements. Compared witois other methods, such as piezoelectric and stepping motors, the VCM has a relatively low-manufacturing cost, while it has an excellent output performance, and can thus be miniaturized. Recently, the market for cameras representing smartphones has been growing, and manufacturers are using these components to implement optical image stabilization (OIS) and auto-focus (AF) functions in camera modules.

The OIS and AF functions are designed to compensate for image and focus instability caused by user hand tremors. When this function was first released, it was mainly used for camera modules at high prices, but it is now commonly used in smartphones and in others devices. This trend is moving toward the size and thickness of the devices containing the modules and the increasing miniaturization of the camera modules. Studies on the miniaturization of actuators for the implementation of OIS and AF functionalities in line with this miniaturized camera module have been conducted as described below.

The following studies and proposals have been conducted for the miniaturization and performance improvement of the entire OIS and camera modules. First, we identified prior studies that attempted optimization simulation using genetic algorithms for the overall size and dimensions of OIS actuators [1], and that also placed magnets and coils on each side of the square-shaped actuators to maximize efficiency in the same space. Similarly, there have been attempts that reduced crosstalk and improved efficiency by adding ferromagnetic objects between coils and magnets [2]. Two magnets of the same size were attached, and the coils were placed at the positions of each pole to confirm the proposal of an actuator that considered the AF and the OIS functionalities [3]. Additionally, an attempt was made to change the arrangement of the coils and magnets within the conventional actuators [4]. Recently, it was also possible to identify the proposed design

The associate editor coordinating the review of this manuscript and approving it for publication was Wei Liu.

of coils by transforming the shape of coils into L-shape [5], conduct the proposed chamming of magnets, and consider the structural studies on both OIS and AF functionalities that can be adjusted in five directions by applying both L-shaped coils and chamfer magnets at the same time.

In addition, new electronic control methods for actuators for OIS could be proposed to increase efficiency [6]. Accordingly, research was conducted to provide electrical signals to enhance OIS and AF functions by adjusting liquid lenses [7] and to study the use of ultrasonic linear motor methods to achieve OIS functionality [8]. These studies and suggestions have been able to identify research trends for VCM actuators for OIS but also for AF.

Various methods have been proposed and applied to date in addition to the aforementioned studies and suggestions to miniaturize and improve performance of VCM actuator camera modules for OIS [9]–[21]. However, it is still difficult to determine how to achieve overall performance, cost, and size (miniaturization). In general, various attempts and possibilities for miniaturization of the module could be confirmed [22]–[42], but it was demonstrated that continuous research is needed in terms of performance improvement and cost reduction.

Reference [9] proposed the chamfer of magnets within the VCM actuator to improve the space efficiency and performance of the camera module. It was confirmed that the proposed method can achieve a similar performance compared with the existing one, while concurrently securing additional space in the module.

In this study, we proposed to improve performance by optimizing the chamfer angle of the magnet inside the VCM actuator and the length of the coil wire diameter at the same time, and to reduce costs using mass production. Based on this proposal, we intended to show that the optimization model leads to additional internal space and improved performance compared with the existing one, and that mass production of the optimal chamfered magnet and coil can reduce the overall manufacturing cost of the OIS VCM actuator.

II. WORKING PRINCIPLE OF OIS MODULE

A. OIS MODULE SELECTION AND WORKING PRINCIPLE CONFIRMATION

The principle of movement of the VCM actuator on the OIS module is that the lens module, including the magnet, is moved along the X- or Y-axes by the Lorentzian force generated by the coil. In this study, the elasticity of the four springs located in each corner section, as shown in Fig. 1(b), was used to enable the module's motion. The lens module can adjust the magnitude (moving distance of the module) of the Lorentzian force in the coil due to the number of windings in the coil, effects of the applied current, type of material in the magnet, and the contact area, according to the principle of electromagnetic induction. Fig. 1(c) shows the that the chamfer magnets and the lens module can move simultaneously from −0.1 mm to +0.1 mm along the X- and Y-axes, respectively.

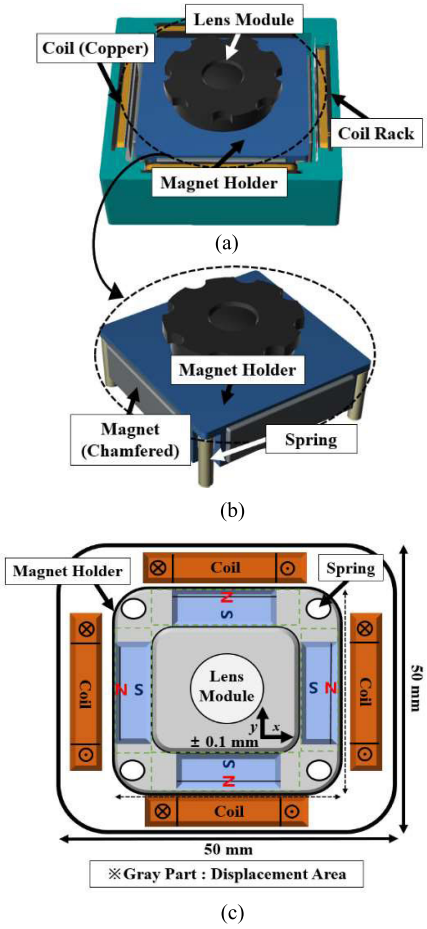

FIGURE 1. (a) Composition of the optical image stabilization (OIS) module. (b) Inner view of the module, (c) top-view (cross-section) and displacement of the lens module.

B. SETTING OF OIS ACTUATOR TYPE AND DESIGN PARAMETERS

As briefly mentioned in the previous section, for the overall structure, the leaf spring structure that is frequently used in camera modules currently sold in the market was applied. The organization of each parameter setup was organized in Table 1, and was designed a) to be approximately five times larger than the camera module that is currently being released for accurate analysis, and b) to increase the connectivity with the OIS module production and experiment.

First, the range of possible displacement of the calculated and manufactured model lens module in the simulation was set to a maximum of 0.2 mm for both the X- and Y-axes. Detailed design parameters for each configuration can be checked from the next section, and the full implementation is shown in Fig. 1(a).

C. ESTABLISHMENT OF THE ENTIRE VERIFICATION PROCESS

In this study, the overall verification configuration, simulation, and experimental design flow are proposed as in Fig. 2. Using the electromagnetic simulation software

TABLE 1. Specifications of the Optical Image Stabilization (OIS) Voice Coil Motor (VCM) Actuator.

Variable	Corresponding Value
Size of proposed VCM actuator	50 mm × 50 mm × 25 mm
Stroke of OIS module	
X-axis direction	-0.1 mm to 0.1 mm
Y-Axis direction	-0.1 mm to 0.1 mm
Magnet	
width	5 mm
depth	30 mm
length	10 mm
(BH) max (MGOe)	43-46
material	Nd-Fe-B N45H
weight	25 g
chamfered degree (variable: θ)	0–30 °
Coil	
width	3.5 mm
depth	35 mm
length	10 mm
wire diameter (variable: d)	0.2–0.25 mm
winding turns	25 turns
material	copper 100% IACS
resistance	15 Ohm
Lens module	
size	40 mm × 40 mm × 25 mm
weight	300 g
Spring	
material	SUS304-WPB
diameter	3 mm
Air gap between magnet and coil	0.15 mm

JMAG Designer and MATLAB, the design and setting of the chamfer magnet angle and coil diameter parameters in the VCM actuator method were conducted, and the Lorentzian force was simulated according to the optimization. At the same time, a mathematical interpretation of the entire camera OIS module applied with it was then linked to produce laboratory-level model. Accordingly, the model was used to measure the motion of the module to which the Lorentzian force was applied according to the chamfer angle of the magnet and the coil diameter of the coil.

The simulation confirmed the Lorentzian force generation for the section between 30° and 0° of the chamfer magnet angle that increased from 0.2 mm to 0.01 mm in increments of 0.2 mm to the maximum value of 0.25 mm, based on the coil diameter. The results corresponding to the optimal point were selected, and an attempt was made to link them to the module's displacement with a numerical approach to the force (Lorentzian force) that occurred in the entire module. When the difference between the Lorentzian force that appeared in the X and Y-axes increased by 10% or more, it was decided to set the specifications of the magnet and coil sets again.

Based on the data obtained at this stage, the camera model was produced. After the installation of the coils for each diameter and the magnets for each chamfer angle, the response speed was checked and selected. Subsequently, the displacements that appeared when currents were applied in the general smartphone printed circuit board (PCB) were measured. If the displacements in the X- and Y-axes differed by more than 10% as in the simulation, the module, coil, and magnet were reconfigured. Finally, comparison of the simulation with the experimental results was based on the overall study flow, as indicated in Fig. 2.

III. CONFIGURATION OF THE OIS MODULE AND SETTING OF MAGNET AND COIL PARAMETERS

A. SETTING OF MAGNET SPECIFICATION

In the case of the magnets, various parameters were determined as shown in Fig. 3(a), and the chamfer angle simulation range maximized the area that faced the coil. To facilitate processing in the experimental models in the future, the chamfer angle was set to range from 0 ° to 30 °. As mentioned earlier, the width, depth, and length of the magnet were adjusted to the overall ratio because the size of the entire camera module was increased five times, and the weight was specified based on the manufacturing specifications. The material of the magnet N45H was designated as Nd-Fe-B. This type is commonly used currently in camera VCM actuators. The position of the chamfer in the magnet section is located on the N pole, and Fig. 1(c) is marked with a solid line.

B. SETTING OF COIL SPECIFICATION

In the case of the coil, various parameters were determined as shown in Fig. 3(b), and the simulation range of the coil diameter was set from 0.2 mm to 0.25 mm. The material was designated as copper, a commonly used material in camera VCM actuators. Because the size of the entire camera module was increased, the width, depth, and length of the coil were also adjusted to the overall ratio. In the case of the diameter, this was determined within the range generally used in current camera VCM actuators. If it was less than 0.2 mm, the allowed current was lowered, and if it exceeded 0.25mm, the number of windings was lowered to less than 20 times, so both cases were excluded.

C. LENS MODULE CONFIGURATION INCLUDING SPRING AND AIR GAP

In the case of lens modules, the shapes were implemented to verify the function of the OIS module, and a magnet holder was implemented on the face where the lens module and the magnet were in contact. The springs at each corner of the lens module were installed as ready-made (commonly used) products, and the air gap was set at 0.15 mm in consideration of the designated movement of the lens module.

IV. ANALYSIS AND OPTIMAL DESIGN OF OIS MODULE

A. SETTING OF SIMULATION DETAILS

In this section, by analyzing the generation of Lorentz force according to the angle of the chamfer magnet, and the diameter of the coil in the structure of the VCM actuator, a simulation was conducted to find the chamfer angle and the coil diameter that can generate the maximum force.

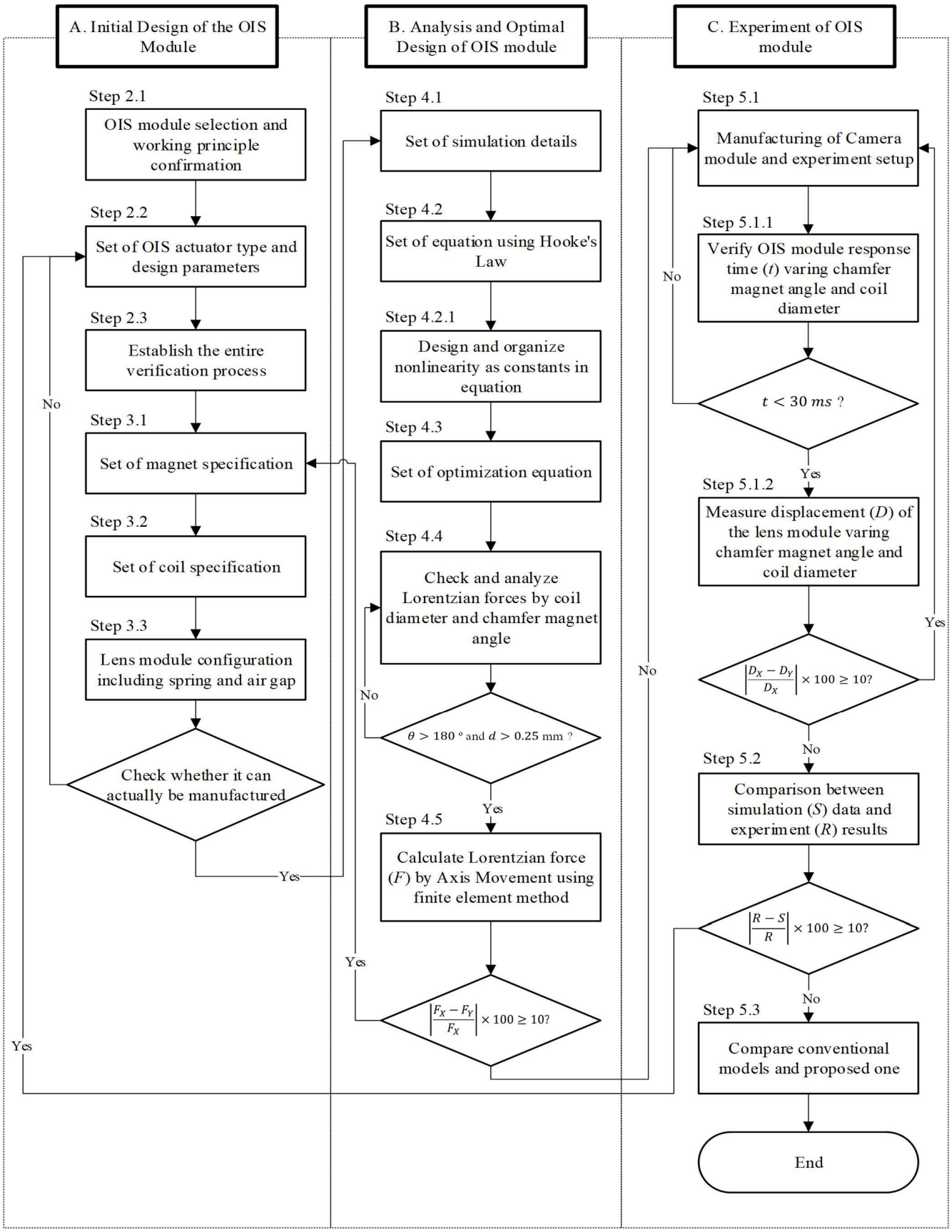

FIGURE 2. The proposed optimal design flow for OIS of camera module.

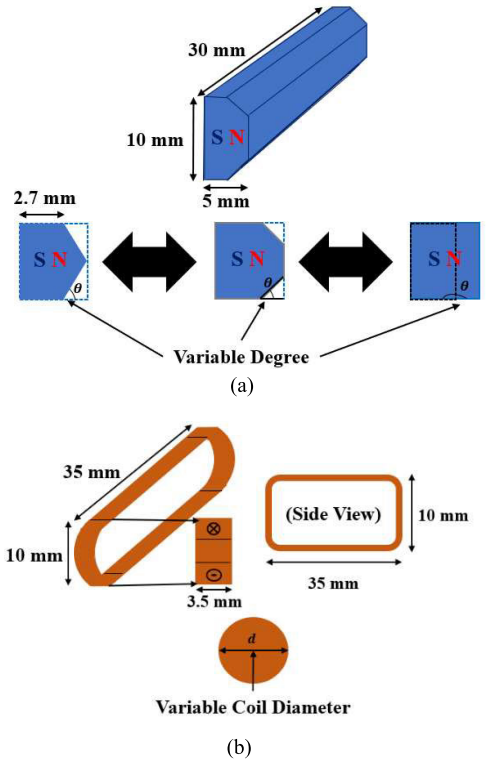

FIGURE 3. (a) Magnet parameters and chamfer angle variable, (b) coil parameters and diameter variable designation.

The parameters of the camera module arranged above were applied equally to the JMAG Designer, and the calculation method was performed using the finite-element-method (FEM). The simulation of the three-dimensional (3D) model implemented based on the arranged contents is shown in Fig. 1(a), and this was applied to JMAG Designer.

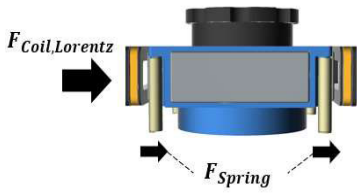

FIGURE 4. Relationship between the spring and the entire module when a Lorentzian force is applied.

B. SETTING OF EQUATION USING HOOKE'S LAW

Analysis using a free-body-diagram (FBD) was conducted on the approach to simulation and subsequent production experiments. To this end, the VCM actuator was simplified to show the force involved, as shown in the 3D modeling figure (Fig. 4). As mentioned above, the simulation and the production camera module prototype in the second half were in the form wherein a total of four springs supported the lens module and the weights of the four magnets. In other words, the weight of the lens module with the magnets ($F_{Lens+Magnet}$) and the elasticity of the four springs (F_{Spring}) were balanced. This can be expressed by the following equation.

$$F_{Lens+Magnet} = F_{spring} \tag{1}$$

When a current is applied to the coil to generate an additional force to move the lens module, the content can be expressed by (2) in accordance with Fig. 4.

$$F_{Coil,Lorentz}+F_{Lens+Magnet} = F_{Spring} \tag{2}$$

In (2), the elastic force of the spring can be expressed by Hooke's law according to (3).

$$F_{Spring} = -kx \tag{3}$$

The elasticity defined by (3) may be expressed by the spring constant and displacement. The displacement here represents the distance the lens module moves on the left and right owing to the Lorentzian force. The force acting on the spring can be considered as a force in the horizontal direction rather than a contraction force in the vertical direction. Accordingly, it can be expressed in the form of (4) based on the addition of a constant in (3) to compensate for it.

$$F_{Spring} = -ckx \tag{4}$$

In (4), the degree to the Lorentzian force that finally occurred in (1) can be confirmed as the displacement (extension) of the spring. Reference was made in a prior study [9], and a prototype was made to measure the relationship between the elastic force of the spring and the Lorentzian force according to the coil diameter and the chamfer magnet angle.

C. SETTING OF OPTIMIZATION EQUATION

As mentioned earlier, in the simulations, the optimization variables were set as the angle of the chamfered of the magnet, the diameter of the coil, expressed according to the following equation.

$$F_{Coil,Lorentz} = w_1 F_{Chamfer\ Degree} + w_2 F_{Coil\ Diameter} \tag{5}$$

Each force F is designated based on the angle of the chamfer of the magnet and the diameter of the coil. In addition, w_1 and w_2 represent the weights (importance). In the case of the two weights, the same value was entered ($w_1 = w_2 = 1$) as the importance was the same, and the maximum value of the Lorentzian force generated in the coil was used as the objective function. Using this optimization function equation, the data of each variable was received, and a simulation was performed to measure the Lorentzian force using the FEM based on the 3D model in Fig. 1.

D. OPTIMAL DESIGN OF OIS MODULE

Fig. 5 is the result of an optimization simulation that graphically shows the Lorentzian force generated for all points based on the angle of the chamfer magnet and the diameter of the coil.

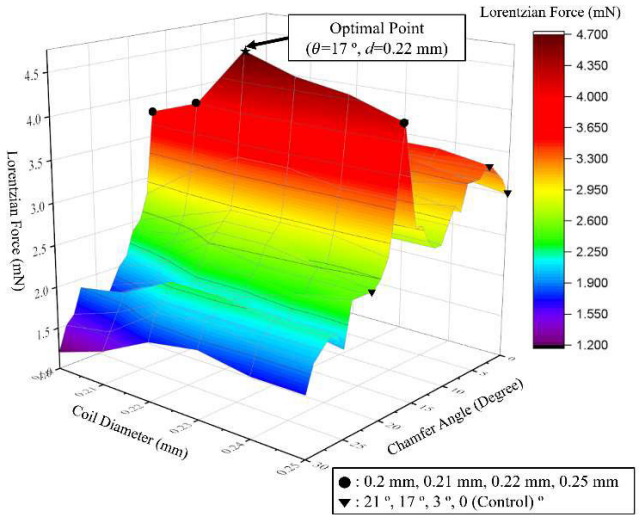

FIGURE 5. Calculated data of the Lorentzian force based on the proposed optimization of the chamfer angle of the magnet and the coil diameter.

The following points can be found in this graph. In the case of the coil diameter, an increase of 0.2 mm to 0.22 mm may increase the Lorentzian force, but in the cases of increases of 0.22 mm or higher, it could be confirmed that the value did not increase but was generally maintained at 0.22 mm.

In the case of the chamfer angle of the magnet, a linear trend was observed based on which the overall Lorentzian force increased as the area became wider from 30 ° in the shape of a triangle to 0 ° in a complete rectangle. In particular, the Lorentzian force that occurred at approximately 17 °, was measured within all sections. That is, it was confirmed that the optimum point of the coil diameter and the chamfer angle of the magnet as a result of the optimization simulation was when the diameter was 0.22 mm and the chamfer angle was 17 °.

E. SIMULATION RESULTS OF DISPLACEMENT

Based on the results obtained from the previous simulations, the results of the Lorentzian forces generated when the lens modules and magnets shown in Fig. 2(c) were displaced from -0.1 mm to 0.1 mm on the X- and Y-axes, respectively. To this end, the coil diameter (the reference when the chamfer angle of the magnet is 17 °) and the chamfer angle of the magnet (the reference when the chamfer angle of the magnet was 0.22 mm) were designated as variables. Accordingly, the degree of influence on the Lorentzian force for each variable could be determined.

Common simulation results in Figs. 6(a) and 6(b) indicate that the Lorentzian force produced by the coils of the lens module and magnet movement along the X- and Y-axes are constant. In Fig. 6(a), when the magnetic chamfer angle was 17 °, the Lorentzian force was maximized. At all other angles, it was observed that as the chamfer angle (30 °) increased, the Lorentzian force decreased. Fig. 6(b) was able to confirm that the Lorentzian force was large when the

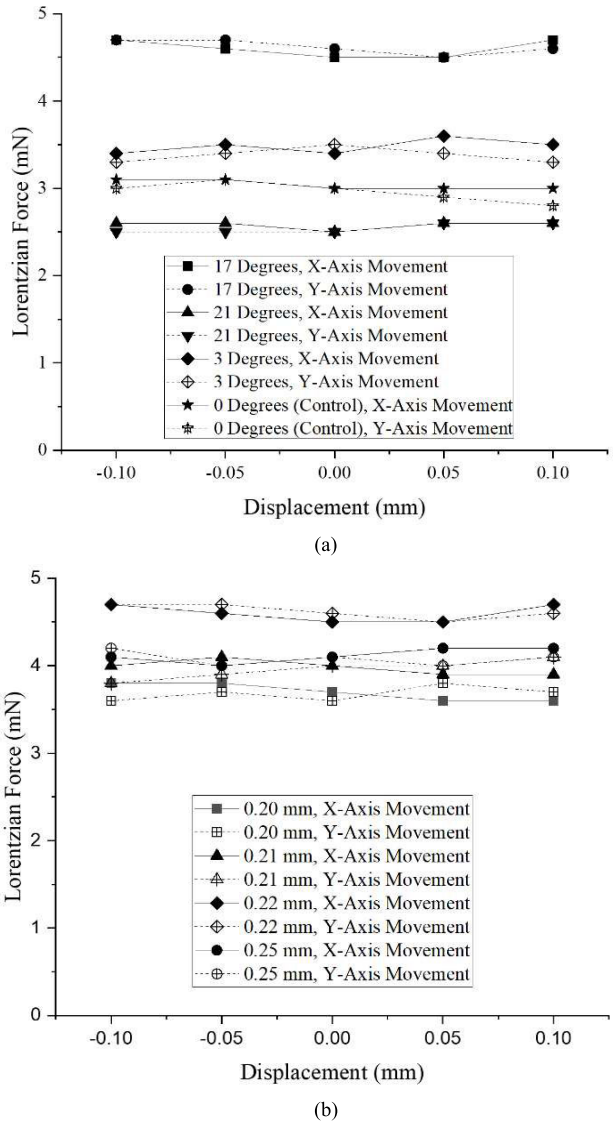

FIGURE 6. Calculated data of the variation of the Lorentzian force when the lens module moved as a function of the (a) angle of chamfer magnet with a coil diameter of 0.22 mm, and as a function of the (b) coil diameter with a chamfer magnet angle of 17 °.

diameter of the coil was 0.22 mm. As the length of the diameter of the coil increased, the Lorentzian force also increased. However, for values from 0.23 mm and above, the same or similar result to that obtained for 0.22 mm was observed.

V. EXPERIMENT OF OIS MODULE

A. MANUFACTURING OF CAMERA MODULE AND EXPERIMENT SETUP

Based on the results obtained according to the aforementioned simulations and numerical analyses, a camera module model was produced and an experiment was conducted.

The model shown in Fig. 7 was made larger than the currently released OIS actuator for clear analysis, and is the same as the VCM actuator specifications applied in the previous simulation. In the configuration of the entire prototype, four

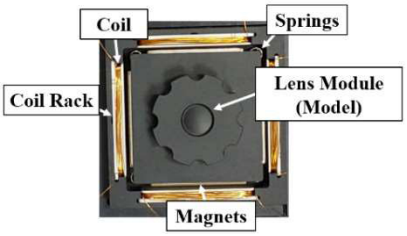

FIGURE 7. The prototype of the proposed OIS system by using a voice coil motor (VCM) for camera module.

magnets can be attached to each side of a square shape on the part in which the lens module was shaped, and four springs that supported and moved them were attached to each corner. The coils were wound 25 times in the direction toward the N pole of the magnet, and a rack existed to maintain the corresponding coil shape.

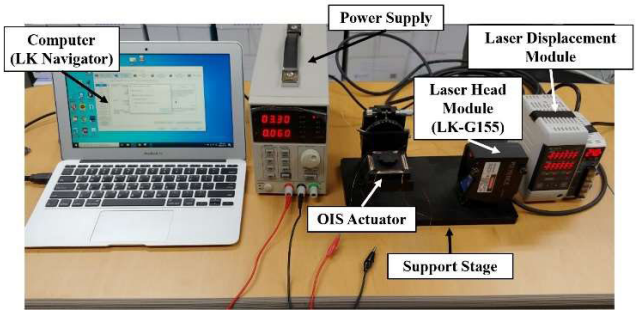

FIGURE 8. Experimental system for the proposed OIS system of camera module.

Fig. 8 shows all necessary equipment for the experiments. The method allows a certain range of current to be applied to the coils mounted on the OIS actuators. When the lens module moved, the laser module and software measures the degree of displacement. The flow chart shows this in Fig. 9.

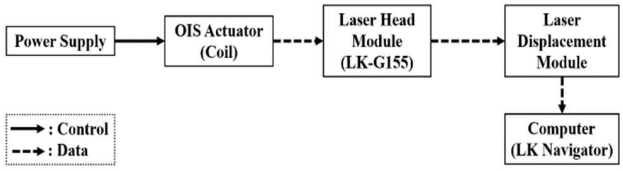

FIGURE 9. Control and data flow throughout the experiment.

Based on the OIS module response time (displacement time 0 mm to 0.04 mm) measurement shown in [9], the magnets and coil were screened by the response time (excluding and reaffirming those that exceeded 30 ms). Additionally, the module's displacement according to the coil diameter was measured based on the optimal chamfer angle of the magnet (equal to 17 °). The module's displacement according to the magnet chamfer angle was measured based on the optimal coil diameter which was equal to 0.22 mm. The applied current was set at 20 mA, as this value is commonly used in the smartphone PCB environment. The coils in which the current flowed through were constructed by winding 25 turns of copper wire, as was done in the simulation. We tried to confirm the optimum magnet chamfer angle and coil diameter using the optimization equation that corresponded to the manufacturing experiment.

B. EXPERIMENTAL RESULTS

After the currents of 20 mA to 60 mA were applied, the displacement of the lens module was measured according to the generated Lorentzian force, and the average values were calculated based on five measurements for each case.

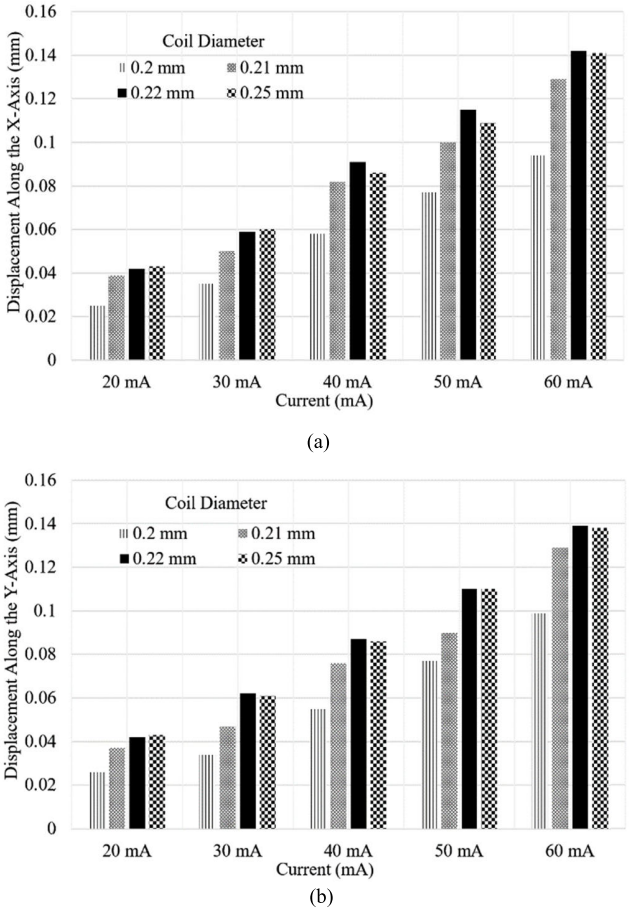

FIGURE 10. Comparison of the displacement of the module based on the coil diameter and current. (a) X-axis movement direction, and (b) Y-axis movement direction based on 17 ° chamfered magnet.

As it can be observed from the previous simulations and graphs in Figs. 10 and 11, the Lorentzian force generated from the coil increased as the current increased. Accordingly, the lens module and the magnet moved. A linear pattern of increasing distance was obtained. In the case of the coil wire diameter in Fig. 10, it was confirmed that the displacement of the module increased linearly as the diameter increased, as indicated in the simulation. However, for lengths from 0.22 mm to 0.22 mm, or higher, there were cases where the value was similar to or greater than 0.22 mm, and both the

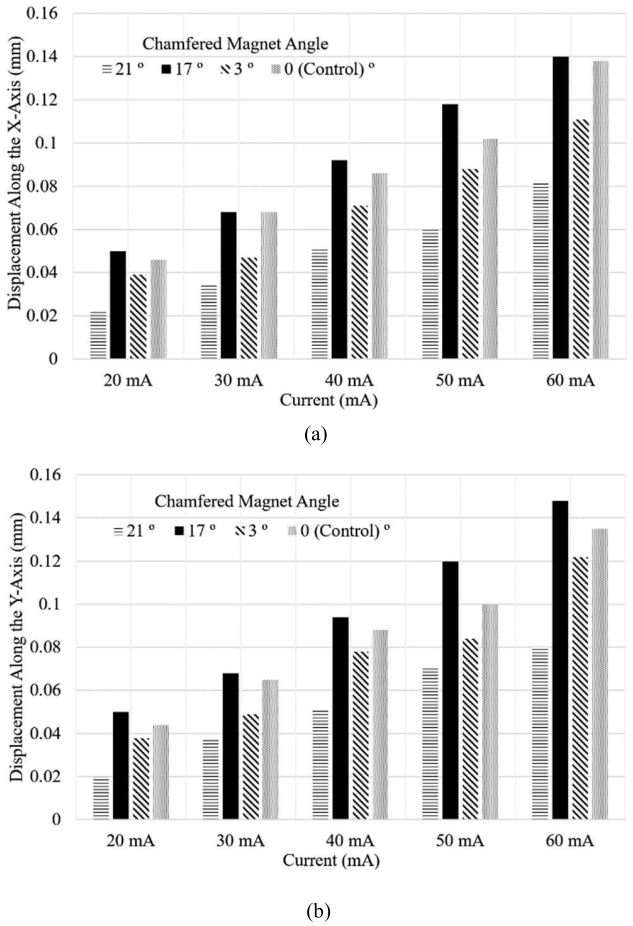

FIGURE 11. Comparison of module's displacement according to the variation of magnet chamfer angle and current. (a) X-axis movement direction, and (b) Y-axis movement direction based on a coil diameter of 0.22 mm.

magnet and coil criteria showed the same tendency when they moved along the X- or Y-axes.

In the case of the chamfered angle of the magnets in Fig. 11, the linear response of the displacement is shown to be increased generally by square (0 °: uncuts), as was shown in the simulations, but the greatest displacement was obtained at the optimum angle of 17 °. Considering the average value, the overall Lorentzian force or displacement that occurred was greater or was at least similar in the case of a chamfer angle of 13 ° compared with the case of the control case (chamfer angle of 0 °).

C. COMPARISON OF CONVENTIONAL MODELS AND PROPOSED ONE

The contents derived from the simulations and experiments conducted thus far are shown in Table 2, and the 'Conventional model' (control group) is based on ratio '1'. Performance is expressed based on the moving distance (displacement), and volume is based on the internal space occupied by magnets and coils. The proposed VCM OIS module indicated how much improvement could be made in terms of performance, volume, and production cost compared to the conventional ones.

TABLE 2. Comparison Between the Conventional Model (CM), the Typical Chamfered Magnet Model (TCM) and the Proposed Optimization Model (POM).

Contents (Ratio)	CM	TCM	POM
Performance (displacement)	1	0.83	1.1
Volume (internal space)	1	0.78	0.77 or less
Production cost	1	0.85 or less	0.85 or less

CM : Conventional model
TCM : Typical chamfered magnet model
POM : Proposed optimization model

1) PERFORMANCE

The conventional VCM OIS modules could even be identified by the use of arbitrary chamfered angle magnets. However, this study even suggested optimization (points) for the chamfered angle of the magnet and the range of the coil diameter, and it was confirmed that the performance was improved by 10% compared to the conventional one. Here, compared with the conventional module of the chamfered angle of the magnet or the diameter of the coil, which is not the optimal point, it was confirmed that the performance was improved by up to 27%.

2) VOLUME

In the conventional VCM OIS modules, two stages were required to drive two axis. However, in this study, 2-Axis was implemented with only one stage. This provides 23% more internal space (volume) than conventional VCM OIS modules. In addition, this can reduce the number of parts such as stage, spring, and others, allowing additional space.

3) PRODUCTION COST

In terms of the overall production cost of the module, By previous implementing two axis with one stage, it is possible to reduce production process by 15% compared to conventional VCM OIS modules by reducing number of parts such as stage and spring. The coil is already manufactured at a low and fixed price as a ready-made product, and 10% of the original price can be reduced in mass production. In the case of magnets, additional processing costs for chamfering are incurred individually, but mass production can offset these additional chamfering processing costs and lower the overall magnet processing cost by up to 10%.

VI. CONCLUSION

According to the fourth industrial revolution and the industrial trend, the demand for small, high-performance, multifunctional camera modules is rapidly increasing. In line with this trend, conventional OIS-related studies have been conducted mainly on specific items such as presentation of deformation shapes of components, miniaturization and optimization of modules. Therefore, the significant value of this research is the proposal of a novel actuator system with OIS

functionality that yielded a high-performance and multifunctional camera module that enabled miniaturization and low cost via a two-axis motional mechanism with a single-stage. Owing to the lack of prior studies on the systematic analysis and optimal design method for actuators for camera modules, this study has important implications given the proposed accurate and rapid analysis and optimal design methods. It is also noteworthy that the proposed methods make it possible to reduce time and cost for the development of actuators for camera modules. This study is also important in that the proposed actuator and its analysis and optimal design method can be applied to various types of electric machines.

REFERENCES

[1] M.-G. Song, Y.-J. Hur, N.-C. Park, K.-S. Park, Y.-P. Park, S.-C. Lim, and J.-H. Park, "Design of a voice-coil actuator for optical image stabilization based on genetic algorithm," *IEEE Trans. Magn.*, vol. 45, no. 10, pp. 4558–4561, Oct. 2009, doi: 10.1109/TMAG.2009.2021399.

[2] J.-H. Woo, J.-H. Yoon, Y. J. Hur, N.-C. Park, Y.-P. Park, and K.-S. Park, "Optimal design of a ferromagnetic yoke for reducing crosstalk in optical image stabilization actuators," *IEEE Trans. Magn.*, vol. 47, no. 10, pp. 4298–4301, Oct. 2011, doi: 10.1109/TMAG.2011.2146237.

[3] Y. H. Chang, C. J. Lu, C. S. Liu, D. S. Liu, and S. H. Chen, "Design of miniaturized optical image stabilization and autofocusing camera module for cell phones," *Sens. Mater.*, vol. 29, no. 7, pp. 989–995, 2017.

[4] C. Kim, M.-G. Song, Y. Kim, N.-C. Park, K.-S. Park, and Y.-P. Park, "Design of a new triple electro-magnetic optical image stabilization actuator to compensate for hand trembling," *Microsyst. Technol.*, vol. 18, nos. 9–10, pp. 1323–1334, Sep. 2012, doi: 10.1007/s00542-012-1538-5.

[5] C.-L. Hsieh, Y.-H. Chang, Y.-T. Chen, and C.-S. Liu, "Design of VCM actuator with L-shape coil for smartphone cameras," *Microsyst. Technol.*, vol. 24, no. 2, pp. 1033–1040, Feb. 2018, doi: 10.1007/s00542-017-3454-1.

[6] W.-Y. Kim, H.-T. Seo, S. Kim, and K.-S. Kim, "Practical approach for controlling optical image stabilization system," *Int. J. Control, Autom. Syst.*, vol. 18, no. 4, pp. 824–833, Apr. 2020, doi: 10.1007/s12555-018-0913-0.

[7] Y.-K. Fuh, J.-K. Chen, and P.-W. Chen, "Characterization of electrically tunable liquid lens and adaptive optics for aberration correction," *Optik*, vol. 126, no. 24, pp. 5456–5459, Dec. 2015, doi: 10.1016/j.ijleo.2015.09.105.

[8] C.-C. Chen, "An optical image stabilization using novel ultrasonic linear motor and fuzzy sliding-mode controller for portable digital camcorders," *IEEE Trans. Consum. Electron.*, vol. 63, no. 4, pp. 343–349, Nov. 2017, doi: 10.1109/TCE.2017.015010.

[9] C.-L. Hsieh, H.-Y. Wang, Y.-H. Chang, and C.-S. Liu, "Design of VCM actuator with the chamfered edge magnet for cellphone," *Microsyst. Technol.*, vol. 23, no. 12, pp. 5293–5302, Dec. 2017, doi: 10.1007/s00542-017-3307-y.

[10] C.-L. Hsieh, C.-S. Liu, and C.-C. Cheng, "Design of a 5 degree of freedom–voice coil motor actuator for smartphone camera modules," *Sens. Actuators A, Phys.*, vol. 309, Jul. 2020, Art. no. 112014.

[11] H.-C. Yu, T.-Y. Lee, S.-K. Lin, L.-T. Kuo, S.-J. Wang, J.-J. Ju, and D.-R. Huang, "Low power consumption focusing actuator for a mini video camera," *J. Appl. Phys.*, vol. 99, no. 8, Apr. 2006, Art. no. 08R901, doi: 10.1063/1.2158927.

[12] L. K. Lai, C. L. Tsai, and T. S. Liu, "Design of compact linear electromagnetic actuator for auto-focusing in phone camera," *IEEE Trans. Magn.*, vol. 47, no. 12, pp. 4740–4744, Dec. 2011, doi: 10.1109/TMAG.2011.2160273.

[13] C.-S. Liu, B.-J. Tsai, and Y.-H. Chang, "Design and applications of novel enhanced-performance force sensor," *IEEE Sensors J.*, vol. 16, no. 12, pp. 4665–4666, Jun. 2016, doi: 10.1109/JSEN.2016.2558661.

[14] H.-K. Lee, N.-J. Choi, S. Jung, K.-H. Park, H. Jung, J.-K. Shim, J.-W. Ryu, and J. Kim, "Electroactive polymer actuator for lens-drive unit in auto-focus compact camera module," *ETRI J.*, vol. 31, no. 6, pp. 695–702, Dec. 2009, doi: 10.4218/etrij.09.1209.0023.

[15] S. Suh, "Stability driven optimal controller design for high quality images," *Electronics*, vol. 7, no. 12, Dec. 2018, Art. no. 437.

[16] P. Pournazari, R. Nagamune, and M. Chiao, "A concept of a magnetically-actuated optical image stabilizer for mobile applications," *IEEE Trans. Consum. Electron.*, vol. 60, no. 1, pp. 10–17, Feb. 2014, doi: 10.1109/TCE.2014.6780919.

[17] Y.-H. Chang, C.-C. Hu, C.-L. Hsieh, and C.-S. Liu, "Design of VCM actuator for optical zooming smartphone cameras," *Microsyst. Technol.*, vol. 25, no. 1, pp. 277–281, Jan. 2019, doi: 10.1007/s00542-018-3962-7.

[18] M.-G. Song, H.-W. Baek, N.-C. Park, K.-S. Park, T. Yoon, Y.-P. Park, and S.-C. Lim, "Development of small sized actuator with compliant mechanism for optical image stabilization," *IEEE Trans. Magn.*, vol. 46, no. 6, pp. 2369–2372, Jun. 2010, doi: 10.1109/TMAG.2010.2042288.

[19] S.-K. Lee and J.-H. Kong, "An implementation of closed-loop optical image stabilization system for mobile camera," in *Proc. IEEE Int. Conf. Consum. Electron. (ICCE)*, Jan. 2014, pp. 45–46.

[20] T. H. Ha, J. Y. Song, C. W. Lee, J. H. Lee, and Y. J. Kim, "Fault diagnosis of VCM type AF actuator module for phone camera by vibration analysis," *Appl. Mech. Mater.*, vol. 459, pp. 125–129, Oct. 2013, doi: 10.4028/www.scientific.net/AMM.459.125.

[21] S. Moon, G. Lee, J. Lee, Y. Park, and M. Yun, "Microactuator for autofocus and optical image stabilization in mobile phone cameras using unleveled comb electrodes," in *Proc. Int. Conf. Opt. Nanophoton.*, Jun. 2016, Art. no. 7565886.

[22] N. Gabdullin and J.-S. Ro, "Energy-efficient eco-friendly zero-holding-Energy magnetic contactor for industrial and vehicular applications," *IEEE Trans. Veh. Technol.*, vol. 69, no. 5, pp. 5000–5011, May 2020, doi: 10.1109/TVT.2020.2981888.

[23] S. S. H. Bukhari, G. J. Sirewal, F. A. Chachar, and J.-S. Ro, "Dual-inverter-controlled brushless operation of wound rotor synchronous machines based on an open-winding pattern," *Energies*, vol. 13, no. 9, p. 2205, May 2020, doi: 10.3390/en13092205.

[24] I. Sami, S. Ullah, Z. Ali, N. Ullah, and J.-S. Ro, "A super twisting fractional order terminal sliding mode control for DFIG-based wind energy conversion system," *Energies*, vol. 13, no. 9, p. 2158, May 2020, doi: 10.3390/en13092158.

[25] S. Madanzadeh, A. Abedini, A. Radan, and J.-S. Ro, "Application of quadratic linearization state feedback control with hysteresis reference reformer to improve the dynamic response of interior permanent magnet synchronous motors," *ISA Trans.*, vol. 99, pp. 167–190, Apr. 2020, doi: 10.1016/j.isatra.2019.08.067.

[26] N. Gabdullin and J.-S. Ro, "Analysis of nonlinear dynamics of permanent magnet magnetic contactor via novel computationally efficient analytical method considering stray and leakage fluxes," *IEEE Access*, vol. 8, pp. 57273–57282, 2020, doi: 10.1109/ACCESS.2020.2982462.

[27] M.-S. Sim and J.-S. Ro, "Semi-analytical modeling and analysis of Halbach array," *Energies*, vol. 13, no. 5, p. 1252, Mar. 2020, doi: 10.3390/en13051252.

[28] S. S. H. Bukhari and J.-S. Ro, "A single-phase line-interactive UPS system for transformer-coupled loading conditions," *IEEE Access*, vol. 8, pp. 23143–23153, 2020, doi: 10.1109/ACCESS.2020.2970489.

[29] J. H. Bang and H. Heo, "Actuator driving device camera module including same," KR Patent 10 2018 0 009 220, Jan. 25, 2018.

[30] S. W. Miller, "Mobile zoom using multiple optical image stabilization cameras," U.S. Patent 2017 0 094 181 A1, Mar. 30, 2017.

[31] K. Min-Su, "Camera module its auto-focusing method," U.S. Patent 2013 0 134 674, Dec. 10, 2013.

[32] S.-J. Kang, "Actuator driving device camera module for mobile device," KR Patent 102 050 106 734, Sep. 22, 2015.

[33] C.-H. Kim, "Camera module," KR Patent 101 804 779, Dec. 5, 2017.

[34] J.-S. Seol and D.-H. Kim, "Camera module actuator," KR Patent 10 2018 0 116 965, Oct. 26, 2018.

[35] J. H. Park, "Actuator for camera module," KR Patent 10 2019 0 114 587, Oct. 10, 2019.

[36] J.-Y. Park and C. M. Park, "OIS camera module and wire spring for OIS camera module," Rbk Emd Co., Gyeonggi-do, South Korea, Tech. Rep. WO2017213359A1, Dec. 2017.

[37] H.-J. Park, H.-K. Yeo, S.-Y. Jung, T.-K. Chung, J.-S. Ro, and H.-K. Jung, "A robust multimodal optimization algorithm based on a sub-division surrogate model and an improved sampling method," *IEEE Trans. Magn.*, vol. 54, no. 3, Mar. 2018, Art. no. 8201704, doi: 10.1109/TMAG.2017.2755073.

[38] J.-W. Kang, H.-J. Park, J.-S. Ro, and H.-K. Jung, "A strategy-selecting hybrid optimization algorithm to overcome the problems of the no free lunch theorem," *IEEE Trans. Magn.*, vol. 54, no. 3, Mar. 2018, Art. no. 8201904, doi: 10.1109/TMAG.2017.2750204.

[39] S.-W. Jung, J.-S. Ro, and H.-K. Jung, "A hybrid algorithm using shape and topology optimization for the design of electric machines," *IEEE Trans. Magn.*, vol. 54, no. 3, Mar. 2018, Art. no. 8102604, doi: 10.1109/TMAG.2017.2764753.
[40] J. Ro, H. Bak, and H. Jung, "Characteristic analysis and design of a novel lorentz force driving actuator for a molded case circuit breaker," *IET Electr. Power Appl.*, vol. 9, no. 1, pp. 1–9, Jan. 2015.
[41] N. Gabdullin, H. Ahmad, and J.-S. Ro, "Next generation autofocus and optical image stabilization system for camera modules using magnetic shape memory actuators," *IEEE Access*, vol. 8, pp. 160177–160187, 2020, doi: 10.1109/ACCESS.2020.3020647.
[42] C.-S. Liu, B. J. Tsai, and Y. H. Chang, "A compact low-cost camera module with modified magnetic restoring force," *J. Mech.*, vol. 33, no. 4, pp. 475–482, Aug. 2017, doi: 10.1017/jmech.2016.121.

TAE-HOON KWON received the B.S. degree from the Department of Electronic Information Engineering, Korea University, Sejong, South Korea, in 2017. He is currently pursuing the master's degree with Chung-Ang University, Seoul, South Korea.

In 2017, he completed an electronic parts course at the Korean Chamber of Commerce and Industry (KCCI), Seoul. From 2017 to 2018, he was with the Research and Development Department related to plasma medical and beauty devices at Prostemics., Company, Ltd., Seoul. His research interests include the design of camera actuators, optimization algorithms, and next-generation transformers.

JONG-SUK RO received his PhD in Electrical Engineering from the Seoul National University (SNU), Seoul, Korea, in 2008 and the B.S. degree in Mechanical Engineering from the Han-Yang University, Seoul, Korea, in 2001.

Currently, he is an Associate Professor of the School of Electrical and Electronics Engineering, Chung-Ang University, Seoul, Korea. In 2014, he was with the University of BATH, Bath, as UK an Academic Visitor. From 2013 to 2016, he worked with the Brain Korea 21 Plus, SNU, as a BK Assistant Professor. He conducted research at the Electrical Energy Conversion System Research Division of the Korea Electrical Engineering & Science Research Institute as a Researcher in 2013. From 2012 to 2013, he was with the Brain Korea 21 Information Technology of SNU, as a Post-Doctoral Fellow. He conducted research at the R&D center of Samsung Electronics as a Senior Engineer from 2008 to 2012. His research interests include the analysis and optimal design of intelligent energy conversion systems such as actuator, generator, and transformer using smart materials such as electromagnetism, piezoelectric, and shape memory alloy.